



Characterizing Neutron-Proton Equilibration in Nuclear Reactions with Subzeptosecond Resolution

A. Jedele,^{1,2,*} A. B. McIntosh,^{1,†} K. Hagel,¹ M. Huang,¹ L. Heilborn,^{1,2} Z. Kohley,^{3,4} L. W. May,^{1,2}
E. McCleskey,¹ M. Youngs,¹ A. Zarrella,^{1,2} and S. J. Yennello^{1,2}

¹Cyclotron Institute, Texas A&M University, College Station, Texas 77843, USA

²Chemistry Department, Texas A&M University, College Station, Texas 77843, USA

³National Superconducting Cyclotron Laboratory, Michigan State University, East Lansing, Michigan 48824, USA

⁴Department of Chemistry, Michigan State University, East Lansing, Michigan 48824, USA

(Received 20 May 2016; published 10 February 2017)

We study neutron-proton equilibration in dynamically deformed atomic nuclei created in nuclear collisions. The two ends of the elongated nucleus are initially dissimilar in composition and equilibrate on a subzeptosecond time scale following first-order kinetics. We use angular momentum to relate the breakup orientation to the time scale of the breakup. The extracted rate constant is 3 zs^{-1} , which corresponds to a mean equilibration time of 0.3 zs. This technique enables new insight into the nuclear equation of state that governs many nuclear and astrophysical phenomena leading to the origin of the chemical elements.

DOI: 10.1103/PhysRevLett.118.062501

The description of atomic nuclei as microscopic liquid drops, proposed in 1935 [1], described the masses of a broad range of nuclides with a simple concept. Subsequently, many liquidlike properties were discovered. For example, viscous forces were seen to play an important role in fission [2] and a boiling transition was observed when nuclei were moderately excited [3]. These and other discoveries motivated the investigation of the nuclear equation of state (NEOS), which describes the relationships between the thermodynamic state variables for a system of strongly interacting dilute nuclear matter ($\rho \geq 10^{11} \text{ g/cm}^3$). The NEOS governs many aspects of astrophysics such as neutron star physics and nucleosynthesis during the explosive death of stars [4–7]. In terrestrial environments, the NEOS is integral in explaining the neutron skin thickness of heavy nuclei, collective excitations of nuclei, and the dynamics of heavy-ion collisions [8–11].

The energy associated with an imbalance of neutrons and protons is termed the symmetry energy, and its density dependence is largely unconstrained. A refined understanding of nuclear material with extreme neutron-proton ratios is necessary, for example, to understand the origin of the elements and characterize the structure and composition of neutron stars. Nuclear scientists across many subfields have contributed to expanding our understanding of the NEOS of neutron-rich and neutron-poor material [12,13]. One method to constrain the symmetry energy involves multi-nucleon exchange between nuclei leading to neutron-proton (n - p) equilibration. Although there has been significant work focused on measuring the asymptotic composition of the nuclei [14–17], some experiments have probed the time scale of the n - p equilibration process. Important efforts in the 1970s and 1980s [18–23] established the time scale is in the range of 0.1–1.0 zs

(1 zeptosecond is 10^{-21} seconds). This was achieved by measuring the isotopic composition of fragments as a function of either the energy dissipation or the separation orientation. The dissipation is related to the interaction time and can be estimated through a model. A recent measurement of a broad range of isotopes and energy dissipation is consistent with this time scale [24]. Similarly, the separation angle is proportional to the interaction time and can be calibrated via angular momentum. Recent measurements by Hudan *et al.* [25–28] employing this technique reported certain fragment compositions explicitly as a function of time, indicating the persistence of the equilibration process for as long as 4 zs, though the majority of the equilibration takes place within 1 zs.

In this Letter, we report direct evidence of n - p equilibration between nuclei on a subzeptosecond time scale. Equilibration chronometry is made possible by applying the method pioneered by Hudan *et al.* [25–28] to experimental data with near-complete angular coverage and excellent isotopic resolution. With the present data, this technique allows us to examine the detailed evolution of the n - p composition of both reaction partners in 0.1 zs time slices.

In the experiment, a beam of ^{70}Zn nuclei was accelerated to 35 MeV/nucleon by the K500 cyclotron at the Texas A&M University Cyclotron Institute. The beam was focused onto a thin foil of ^{70}Zn (95% pure). The nuclear reaction products were measured in NIMROD (Neutron Ion Multidetector for Reaction Oriented Dynamics) [29], which provides nearly complete geometrical coverage (3.6° to 167.0° relative to the beam axis). NIMROD provides excellent isotopic identification of charged particles up to $Z = 17$ in most detectors, and up to $Z = 21$ in some detectors [30,31]. Elemental identification is achieved up

through $Z = 30$ (atomic number of beam). The combination of the isotopic resolution and the full geometric coverage are crucial to observing the time dependence of the n - p equilibration with high resolution. In contrast to previous work where the lighter fragment of a binary split was measured and interpreted as demonstrating equilibration with its heavier partner, in this work we make the simultaneous measurement of both reaction partners of a binary split, conclusively demonstrating observation of the equilibration process.

Heavy-ion reactions in this energy regime produce an excited projectilelike fragment (PLF*) and an excited targetlike fragment (TLF*). As the PLF* and TLF* begin to move apart after colliding, a neck of nuclear material is formed between them as illustrated in Fig. 1(a). The system is strongly elongated by the collision dynamics, and is stretched beyond the capabilities of the attractive nuclear force to hold it together. As a result, the neck ruptures and the emerging PLF* and TLF* are typically strongly deformed along their axis of separation (\vec{v}_{CM}) [32–34]. Figure 1(b) depicts the deformation of the two fragments shortly after the neck rupture and prior to subsequent breakup. Because of the deformation, the PLF* and TLF* are likely to break up promptly along the deformation axis. These types

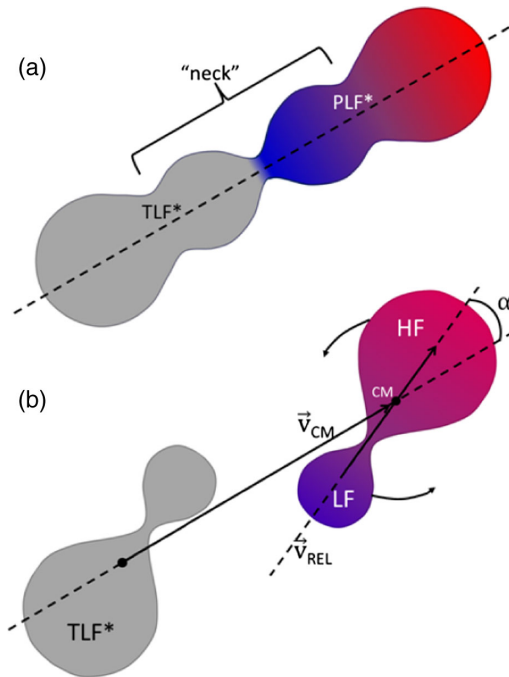


FIG. 1. Illustration of dynamical deformation and decay. Panel (a) shows the deformed PLF* and TLF* system before rupture of the neck. Panel (b) shows a later time after the PLF* and TLF* system has separated. The PLF* has rotated relative to the TLF* separation axis (\vec{v}_{CM}) and is itself about to break up into two fragments (**HF** and **LF**). The time the PLF* lives before breaking up is measured by the angle α . The color denotes the composition with blue indicating neutron richness and red indicating relative neutron deficiency.

of breakups, referred to as dynamical decay, exhibit a characteristic angular distribution peaked along the beam direction [34–36]. Because our detectors are optimized to measure the fragments of the PLF* with high efficiency, we focus on the PLF* decay with the understanding that the same process occurs for the TLF* [33]. Since the fragments of the TLF* are not measured, they are represented as gray in the cartoon. The coloring of the PLF* reflects the measured composition, which will be discussed later.

In order to focus on the dynamical decay of the PLF*, we selected events in which at least two charged particles were measured in NIMROD. Fragments were sorted by their atomic number with charge-identical fragments sorted by mass number. We refer to the fragment with the largest atomic number as the heavy fragment (**HF**) and the fragment with the second largest atomic number as the light fragment (**LF**). The **HF** was required to have an atomic number of $Z_H \geq 12$, and **LF** was required to have an atomic number of $Z_L \geq 3$. We also require a total measured charge of $21 \leq Z_{\text{tot}} \leq 32$, which includes Z_H , Z_L , and all other charged fragments measured. These requirements maximize the likelihood that these two fragments are the heaviest two daughters of the PLF*. Finally, we require that both the **HF** and **LF** be isotopically identified. Evidence that both the **HF** and **LF** originate from the PLF* is seen in the velocity distributions [31]: both fragments are centered above midvelocity as illustrated in Fig. 1, and consistent with previous work [34].

To examine the strong alignment expected from dynamical decays of a deformed PLF*, we look at the distribution of the alignment angle $\alpha = \arccos[\vec{v}_{\text{CM}} \cdot \vec{v}_{\text{REL}} / (|\vec{v}_{\text{CM}}| |\vec{v}_{\text{REL}}|)]$. The velocity vectors represent the two-fragment center-of-mass velocity $\vec{v}_{\text{CM}} = (m_{\text{HF}}\vec{v}_{\text{HF}} + m_{\text{LF}}\vec{v}_{\text{LF}}) / (m_{\text{HF}} + m_{\text{LF}})$ and the relative velocity $\vec{v}_{\text{REL}} = \vec{v}_{\text{HF}} - \vec{v}_{\text{LF}}$. These quantities are illustrated in Fig. 1(b). After the neck rupture, and as they move apart along their separation axis (the direction of \vec{v}_{CM}) the PLF* and TLF* continue to rotate and their shapes continue to evolve. A later point in time is shown in panel (b) when the PLF* is about to split into two fragments (**HF** and **LF**). The lifetime of the PLF*, after breaking from the TLF* and before breaking into the **HF** and **LF**, is correlated with the rotation angle α [depicted in panel (b)]. Thus the equilibration chronometry technique utilizes \vec{v}_{CM} and \vec{v}_{REL} to define the orientation of the PLF* at those two critical points in time, and the angle made by these vectors can then be related to its lifetime. By this definition, $\alpha = 0^\circ$ corresponds to $t = 0$ with the **LF** emitted in the backward direction relative to the **HF**, and larger rotations correspond to longer time.

Selected angular distributions, $\cos(\alpha)$, are shown in Fig. 2. The upper left panel of Fig. 2 ($Z_H = 14$, $Z_L = 5$) shows a large peak near $\cos(\alpha) = 1$. The peak extends with significant yield out to $\cos(\alpha) = 0.5$. Beyond this, the yield becomes relatively flat, but displays a slight

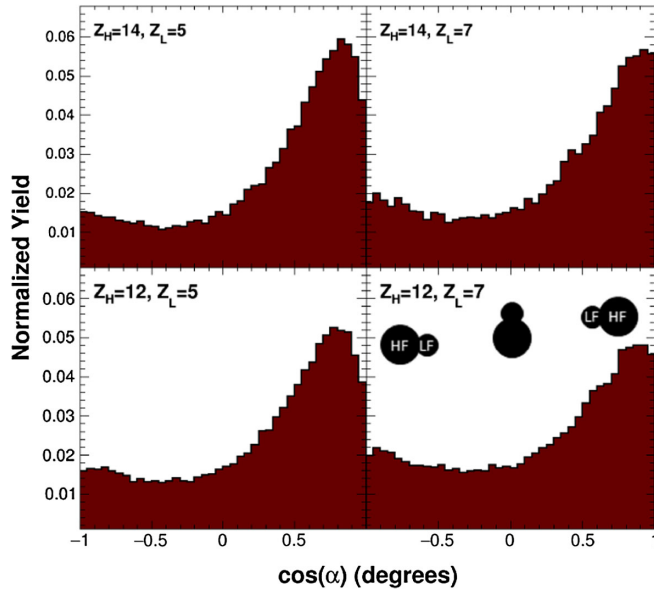


FIG. 2. Normalized angular distributions for select Z_H and Z_L pairings. Emission of the lighter charged fragment in the backward direction (toward the target) corresponds to $\cos(\alpha) = 1$.

excess near $\cos(\alpha) = -1$. This trend is seen as well in the other three panels ($Z_H = 14, Z_L = 7$; $Z_H = 12, Z_L = 5$; and $Z_H = 12, Z_L = 7$). These pairings were selected to examine the impact of varying Z_H and Z_L independently. Forty-three pairings were analyzed, with Z_H ranging from 12 to 19 and Z_L ranging from 3 to 11. Those shown represent a good compromise between a significant variation in (Z_H, Z_L) and high statistics, and are representative of the entire set. The similarities for the angular distributions indicate the same basic reaction dynamics.

To understand the observed yield we consider two mechanisms of production: statistical decay and dynamical decay. For statistical decay from a nonrotating source, the angular distribution should be flat as a function of $\cos(\alpha)$. With rotation, the distribution evolves to have increased yield at $\cos(\alpha) = \pm 1$ due to the tendency to decay in the plane perpendicular to the angular momentum vector. The larger the angular momentum, the greater the yield at $\cos(\alpha) = \pm 1$, though symmetry about $\cos(\alpha) = 0$ would be maintained. The observed yield for $\cos(\alpha) < 0$ may therefore be due primarily to statistical decay. The effect of the measurement device on the symmetry of the angular distribution was investigated using the statistical model GEMINI++ [37]. The simulation was filtered with a NIMROD array simulation environment. The granularity, resolution, and thresholds of the detection device preserve the symmetry of the angular distribution for statistical decay. Hence, the larger yield for $\cos(\alpha) > 0$ seen in Fig. 2 cannot be ascribed to purely statistical decay.

The excess yield for $\cos(\alpha) > 0$ is consistent with dynamical decay: the breakup of the PLF* tends to occur aligned with the separation axis of the PLF*-TLF* breakup.

The angular distribution is therefore peaked for the most aligned configuration, $\cos(\alpha) = 1$, and decreases in yield with decreasing alignment. This excess yield is largest and most strongly aligned for the most asymmetric splits (Fig. 2, left panels: $Z_H = 14, Z_L = 5$; and $Z_H = 12, Z_L = 5$). For more symmetric pairings, the preference for strongly aligned backward emission decreases slightly, as seen by the decrease in the peak value of the normalized yield and slight broadening of the distribution from (top left panel: $Z_H = 14, Z_L = 5$) to (bottom right panel: $Z_H = 12, Z_L = 7$), in agreement with previous studies of dynamical decay [34]. This may be understood in terms of a large collectivity and larger potential barrier slowing the symmetric splits and decreasing their likelihood. This provides support that the **HF** and **LF** are produced dynamically. The time scale of dynamical decays of the PLF*, evident in Fig. 2, is short relative to PLF* rotation time. Less aligned decays represent longer times. This is the basis for using the rotation of the dinuclear system as a clock.

For each pairing of (Z_H, Z_L) , the asymmetry $\langle \Delta \rangle = \langle N - Z/A \rangle$ was calculated as a function of the alignment angle (α) for both the **HF** and for **LF**. Figure 3 shows $\langle \Delta \rangle$ distributions for the same (Z_H, Z_L) pairings shown in Fig. 2. The large number of angular bins afforded by the experimental configuration allows the evolution of $\langle \Delta \rangle$ to be examined in detail. For the **LF**, a large initial $\langle \Delta_L \rangle$ value is seen (at $\alpha = 0^\circ, t = 0$), followed by a sharp decrease in $\langle \Delta_L \rangle$ for small angles of rotation. After the initial decrease, $\langle \Delta_L \rangle$ levels off. Complementarily, $\langle \Delta_H \rangle$ starts at a small value, initially rises, and slows its ascent at a rate similar to that of $\langle \Delta_L \rangle$. The evolution of $\langle \Delta_L \rangle$ and $\langle \Delta_H \rangle$ with

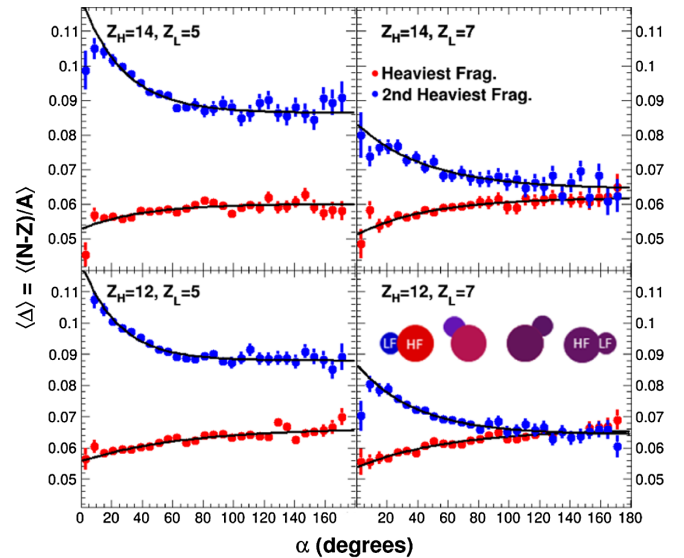


FIG. 3. Composition as a function of decay alignment showing equilibration. As the angle of rotation increases (α increases from 0° to 180°), the $\langle N - Z/A \rangle$ initially decreases rapidly for Z_L and increases for Z_H before plateauing. The majority of equilibration occurs between 0° and 80° .

alignment appears exponential, suggesting first-order kinetics. The evolution of the composition is illustrated by the inset in Fig. 3 and by the coloring in Fig. 1, using blue to indicate a neutron abundance and red to indicate a relative neutron deficiency.

To understand the origin of these features, consider the dynamical mechanism. Because of the dynamical deformation of the PLF* and presence of a velocity gradient, the PLF* tends to quickly break into two pieces along the direction of deformation. The material near midvelocity, i.e., the neck connecting the PLF* and TLF*, is neutron rich due to preferential flow of the neutrons to this region of low density [38]. This flow occurs as the system seeks to minimize the symmetry energy. If very prompt decay occurs then the composition of the **LF**, which originates near the neck region, will be neutron rich, and the **HF** will be neutron poor to compensate. However, the attractive nuclear force has a chance to delay or even prevent dynamical decay; surface tension drives the strongly deformed PLF* toward sphericity. While these regions of the PLF* are in contact, their densities may evolve toward each other, allowing their asymmetries to do likewise. Thus a slower decay (farther from $\alpha = 0^\circ$) ought to exhibit more similar values of $\langle\Delta_H\rangle$ and $\langle\Delta_L\rangle$.

The plateau values seen in Fig. 3 are not necessarily equal. The thermodynamic equation of state indicates that the **HF** and **LF** should approach a common chemical potential rather than a common composition. The chemical potentials are dependent on variations in internal energy, density and ground-state binding energies; the conversion from composition to chemical potential is not trivial. The composition is directly measurable and model independent.

We explored the effects of secondary decay within GEMINI++. Secondary decay causes a modest decrease of the Δ values, and a slight reduction in the range of Δ . However, the exponential trend is neither created nor destroyed by secondary decay, and the rate constant of the exponential is not affected within experimental uncertainty.

The change in $\langle\Delta_L\rangle$ is larger than the change in $\langle\Delta_H\rangle$ (Fig. 3) due to mass conservation. Since Z_H is larger, exchanging nucleons affects $\langle\Delta_L\rangle$ more than $\langle\Delta_H\rangle$.

To study the equilibration kinetics, the dependence of $\langle\Delta_H\rangle$ and $\langle\Delta_L\rangle$ on α was parameterized by the form $\langle\Delta\rangle = a + b \cdot \exp(-c\alpha)$. The results of the fits are shown as the black curves in Fig. 3. The exponential form describes the experimental data well, confirming first-order kinetics. The parameter c is a surrogate for the equilibration rate constant. It is a direct measure of the exponential slope of the composition with respect to rotation angle. The rate constants for all eight curves shown in Fig. 3 are equal within experimental uncertainty. This consistency holds true for all 43 pairings analyzed. The average rate constant was 0.02 ± 0.01 per degree for the **HF** and 0.03 ± 0.01 per degree for the **LF**. The rate constant for the **HF** is

independent of Z_L , and the rate constant for the **LF** is independent of Z_H . The agreement of rate constants within experimental uncertainty indicates that the force driving the equilibration is independent of the size of both partners, and only depends on the difference in asymmetry, or, more accurately, on the difference in chemical potential.

If the correlation between rotation angle and decay time is monotonic (i.e., decay time is short relative to rotation period), then c is a good surrogate for the rate constant. Strong evidence of this exists in the angular anisotropy seen in Fig. 2; if decay time were not significantly shorter than rotational period, the angular distribution would appear isotropic. By making the assumption that the correlation between rotation angle and decay time is linear, then c can be used to find a true rate constant in units of inverse time rather than inverse angle. The time scale is determined through $t = \alpha/\omega$, where t is time and ω is angular frequency. The angular frequency is dependent on the angular momentum (J) and moment of inertia (I_{eff}): $\omega = (J\hbar)/I_{\text{eff}}$. The moment of inertia is calculated for a system of two touching spheres, the **HF** and **LF**, rotating around their common center of mass: $I_{\text{eff}} = m_H r_{\text{CM},H}^2 + \frac{2}{5} m_H r_H^2 + m_L r_{\text{CM},L}^2 + \frac{2}{5} m_L r_L^2$. Here, r_H is the radius of the **HF**, r_L is the radius of the **LF**, $r_{\text{CM},H}$ is the distance from the center of the **HF** to the two-fragment center-of-mass, and $r_{\text{CM},L}$ is the distance from the center of the **LF** to the two-fragment center-of-mass. The masses of **HF** and **LF** are denoted by m_H and m_L , respectively. The moment of inertia ranged from $2.8\text{--}9.9 \times 10^{-42}$ MeV \cdot s² for different combinations of the **HF** and **LF**, but contributes little uncertainty for any given pairing.

The angular momentum was determined using the width of the out-of-plane α -particle distribution. Fission studies [39] have shown the out-of-plane fragment distribution width is proportional to the angular momentum of the parent nucleus. In this case, the parent is the combined **HF** and **LF** system. The spin axis is perpendicular to the reaction plane, defined by the beam axis and the two-fragment center-of-mass velocity vector \vec{v}_{CM} . For alpha particles measured in coincidence with any **HF** and **LF** pair, the angle ϕ relative to this reaction plane is calculated. Figure 4 shows the experimental distribution of $\sin(\phi)$ in blue. The width of the measured distribution, 0.28, is sensitive to the angular momentum of the parent. The detector efficiency impacts the central four bins, but doesn't impact the width of the distribution. The distribution has only negligible variation for different (Z_H , Z_L) combinations. Comparison of the distribution of forward emitted alpha particles to Fig. 4 indicates that our assessment of J is robust with respect to strong deformation of the PLF*. We use the GEMINI++ model to assess the angular momentum. The experimental distribution may be reproduced for a variety of angular momenta and excitation energies. A spin of $10\hbar$ can reproduce the width of $\sin(\phi)$ for low excitation energy ($E^*/A = 0.8$ MeV). A spin of $50\hbar$ can reproduce

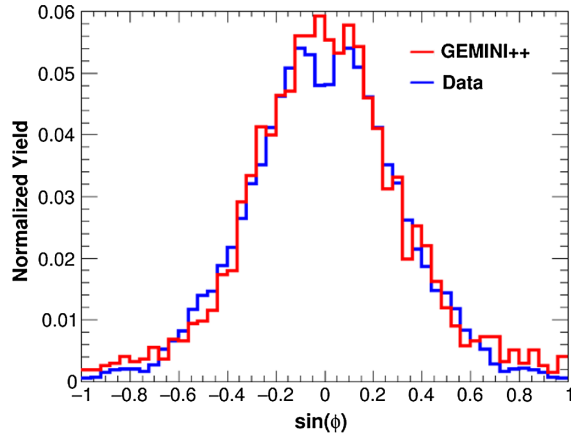


FIG. 4. Out-of-plane α -particle distribution comparing experimental data and the GEMINI++ model to evaluate the spin ($22\hbar$).

the width of $\sin(\phi)$ for higher excitation ($E^*/A = 1.2$ MeV). Beyond this range, it is difficult to justify higher angular momentum transfer or lower excitation energy. Taking the geometric mean of the extremes of the range in spin, we obtain $22\hbar$ with a factor of 2.2 systematic uncertainty. The resulting angular distribution at $22\hbar$ from GEMINI++ is shown by the red line in Fig. 4. From this, we calculate rotational periods ranging from 1 to 4 zs, with an average of $3 \pm_1^6$ zs. The calculated time scales, rate constants and mean lifetimes are shown in Table I. Details may be found in Ref. [31].

We have examined binary decay of deformed, out-of-equilibrium nuclei. The composition of the daughters exhibits a smooth evolution over time. The time scale is directly probed with the angular distribution by taking advantage of the fact that the decay occurs on a fraction of the rotation time scale. With this measurement, we demonstrate the power of this experimental technique for measuring n - p equilibration in action. The examination of the time dependence of the equilibration provides a direct connection to the nuclear equation of state. A previously unobserved consequence of the nuclear equation of state is now demonstrated using this technique: namely, that the equilibration of neutrons and protons in nuclear matter follows first-order kinetics. The rate constant is around 3 zs^{-1} , which corresponds to a mean lifetime of equilibration of 0.3 zs.

TABLE I. Extracted parameters quantifying the rate of n - p equilibration.

Z_H, Z_L	Pairing	Period (zs)	k_H (zs^{-1})	k_L (zs^{-1})	τ_H (zs)	τ_L (zs)
12, 5		$2 \pm_1^5$	$3 \pm_1^3$	$7 \pm_4^9$	$0.4 \pm_{0.2}^{0.7}$	$0.1 \pm_{0.1}^{0.3}$
12, 7		$3 \pm_1^6$	$2 \pm_1^3$	$4 \pm_2^4$	$0.5 \pm_{0.2}^1$	$0.3 \pm_{0.1}^{0.6}$
14, 5		$2 \pm_1^5$	$4 \pm_3^5$	$6 \pm_3^7$	$0.3 \pm_{0.1}^{0.6}$	$0.2 \pm_{0.1}^{0.4}$
14, 7		$3 \pm_1^7$	$3 \pm_2^3$	$3 \pm_2^3$	$0.4 \pm_{0.2}^{0.9}$	$0.4 \pm_{0.2}^{0.8}$
Average		$3 \pm_1^6$	$3 \pm_2^4$	$4 \pm_2^4$	$0.3 \pm_{0.2}^{0.7}$	$0.3 \pm_{0.1}^{0.6}$

In 2004, Tsang *et al.* [14] published nucleon transport simulations that displayed sensitivity of n - p equilibration to the form of the density dependence of the symmetry energy employed in the model. A plot of the composition of the reaction partners changing in time illustrated that equilibration depends on the contact time, the potential driving equilibration, and relative n - p asymmetry of the reaction partners. Subsequent research focused on how the final-state nuclear compositions might be used to constrain the equation of state rather than on measuring the time dependence of the equilibration. However, the time dependence carries more information about the NEOS than the final-state values, and our current results demonstrate that this can be observed with the proper tools. This new data, and the new avenue of experimental research it opens up, will guide theoretical developments in nuclear science. These advances promise to deepen our understanding of the fundamental interactions of nuclear material.

This work was made possible by support from the DOE (DE-FG02-93ER40773) and the Robert A. Welch Foundation (A-1266). We thank the staff of the TAMU Cyclotron Institute for the excellent particle beams and technical support. We gratefully acknowledge Kyle Brown, Sylvie Hudan, Joe Natowitz, and Lee Sobotka for critical reading of the manuscript. We would further like to thank Robert Charity for use of GEMINI++ code.

*ajedele@comp.tamu.edu

†alan.b.mcintosh@gmail.com

- [1] C. F. v. Weizsäcker, Zur Theorie der Kernmassen, *Zeitschrift für Physik* **96**, 431 (1935).
- [2] K. T. R. Davies, A. J. Sierk, and J. R. Nix, Effect of viscosity on the dynamics of fission, *Phys. Rev. C* **13**, 2385 (1976).
- [3] V. Viola and K. Kwiatkowski, How to boil a nucleus, *Am. Sci.* **86**, 449 (1998).
- [4] P. B. Demorest, T. Pennucci, S. M. Ransom, M. S. E. Roberts, and J. W. T. Hessels, A two-solar-mass neutron star measured using Shapiro delay, *Nature (London)* **467**, 1081 (2010).
- [5] A. W. Steiner, M. Prakash, J. M. Lattimer, and P. J. Ellis, Isospin asymmetry in nuclei and neutron stars, *Phys. Rep.* **411**, 325 (2005).
- [6] J. M. Lattimer and M. Prakash, Neutron star structure and the equation of state, *Astrophys. J.* **550**, 426 (2001).
- [7] J. M. Lattimer and M. Prakash, The physics of neutron stars, *Science* **304**, 536 (2004).
- [8] U. Garg *et al.*, The giant monopole resonance in the Sn isotopes: Why is tin so fluffy?, *Nucl. Phys.* **A788**, 36 (2007).
- [9] P. Danielewicz, R. Lacey, and W. G. Lynch, Determination of the equation of state of dense matter, *Science* **298**, 1592 (2002).
- [10] V. Baran, M. Colonna, M. Di Toro, A. Croitoru, and A. I. Nicolini, Mass and isospin dependence of the dipole response in a microscopic transport approach, *AIP Conf. Proc.* **1645**, 267 (2015).

- [11] X. Roca-Maza, M. Centelles, X. Viñas, and M. Warda, Neutron Skin of Radius Experiment, *Phys. Rev. Lett.* **106**, 252501 (2011).
- [12] C. J. Horowitz, E. F. Brown, Y. Kim, W. G. Lynch, R. Michaels, A. Ono, J. Piekarewicz, M. B. Tsang, and H. H. Wolter, A way forward in the study of the symmetry energy: experiment, theory, and observation, *J. Phys. G* **41**, 093001 (2014).
- [13] M. B. Tsang *et al.*, Constraints on the symmetry energy and neutron skins from experiments and theory, *Phys. Rev. C* **86**, 015803 (2012).
- [14] M. B. Tsang *et al.*, Isospin Diffusion and the Nuclear Symmetry Energy in Heavy Ion Reactions, *Phys. Rev. Lett.* **92**, 062701 (2004).
- [15] D. V. Shetty, S. J. Yennello, and G. A. Souliotis, Density dependence of the symmetry energy and the nuclear equation of state: A dynamical and statistical model perspective, *Phys. Rev. C* **76**, 024606 (2007).
- [16] Z. Y. Sun *et al.*, Isospin diffusion and equilibration for Sn + Sn collision at $E/A = 35$ MeV, *Phys. Rev. C* **82**, 051603 (2010).
- [17] L. May, Isospin Equilibration in Fermi-Energy Heavy-Ion Nuclear Collisions, PhD thesis, Texas A&M University, 2015, <http://hdl.handle.net/1969.1/155699>.
- [18] J. Galin, B. Gatty, D. Guerreau, M. Lefort, X. Tarrago, R. Babinet, B. Cauvin, J. Girard, and H. Nifenecker, The transition between quasi elastic and completely damped collisions studied in the ^{40}Ar (280 MeV) + ^{58}Ni reaction, *Z. Phys. A* **278**, 347 (1976).
- [19] J. V. Kratz, H. Ahrens, W. Bögl, W. Bröchle, G. Franz, M. Schädel, I. Warnecke, G. Wirth, G. Klein, and M. Weis, Charge-Asymmetry Equilibration in the Reaction of $^{129,132,136}\text{Xe}$ with ^{197}Au Near the Interaction Barrier, *Phys. Rev. Lett.* **39**, 984 (1977).
- [20] L. G. Moretto and R. P. Schmitt, Deep inelastic reactions: a probe of the collective properties of nuclear matter, *Rep. Prog. Phys.* **44**, 533 (1981).
- [21] E. S. Hernandez, W. D. Myers, J. Randrup, and B. Remaud, Quantal dynamics of charge equilibration in damped nuclear collisions, *Nucl. Phys.* **A361**, 483 (1981).
- [22] G. J. Matthews, J. B. Moulton, G. J. Wozniak, B. Cauvin, R. P. Schmitt, J. S. Sventek, and L. G. Moretto, ^{20}Ne -induced reactions with Cu and ^{197}Au at 8.6 and 12.6 MeV/nucleon, *Phys. Rev. C* **25**, 300 (1982).
- [23] H. Freisleben and J. V. Kratz, N/Z -equilibration and nucleon exchange in dissipative heavy-ion collisions, *Phys. Rep.* **106**, 1 (1984).
- [24] G. A. Souliotis, P. N. Fountas, M. Veselsky, S. Galanopoulos, Z. Kohley, A. McIntosh, S. J. Yennello, and A. Bonasera, Isoscaling of heavy projectile residues and N/Z equilibration in peripheral heavy-ion collisions below the Fermi energy, *Phys. Rev. C* **90**, 064612 (2014).
- [25] S. Hudan *et al.*, Tracking saddle-to-scission dynamics using N/Z in projectile breakup reactions, *Phys. Rev. C* **86**, 021603 (2012).
- [26] K. Brown, S. Hudan, R. T. deSouza, J. Gauthier, R. Roy, D. V. Shetty, G. A. Souliotis, and S. J. Yennello, Timescale for equilibration of N/Z gradients in dinuclear systems, *Phys. Rev. C* **87**, 061601 (2013).
- [27] K. Stiefel, Z. Kohley, R. T. deSouza, S. Hudan, and K. Hammerton, Symmetry energy dependence of long-timescale isospin transport, *Phys. Rev. C* **90**, 061605 (2014).
- [28] S. Hudan and R. T. deSouza, Timescale for isospin equilibration in projectile breakup, *Eur. Phys. J. A* **50**, 36 (2014).
- [29] S. Wuenschel, K. Hagel, R. Wada, J. B. Natowitz, S. J. Yennello, Z. Kohley, C. Bottosso, L. W. May, W. B. Smith, D. V. Shetty, B. C. Stein, S. N. Soisson, and G. Prete, NIMROD-ISiS, a versatile tool for studying the isotopic degree of freedom in heavy ion collisions, *Nucl. Instrum. Methods Phys. Res., Sect. A* **604**, 578 (2009).
- [30] Z. Kohley *et al.*, Investigation of transverse collective flow of intermediate mass fragments, *Phys. Rev. C* **82**, 064601 (2010).
- [31] See Supplemental Material at <http://link.aps.org/supplemental/10.1103/PhysRevLett.118.062501> for critical analysis details.
- [32] C. P. Montoya *et al.*, Fragmentation of Necklike Structures, *Phys. Rev. Lett.* **73**, 3070 (1994).
- [33] J. Colin *et al.*, Dynamical effects in multifragmentation at intermediate energies, *Phys. Rev. C* **67**, 064603 (2003).
- [34] A. B. McIntosh *et al.*, Short-lived binary splits of an excited projectilelike fragment induced by transient deformation, *Phys. Rev. C* **81**, 034603 (2010).
- [35] F. Bocage *et al.*, Dynamical effects in nuclear collisions in the Fermi energy range: Aligned breakup of heavy projectiles, *Nucl. Phys.* **A676**, 391 (2000).
- [36] B. Davin *et al.*, Fragment production in noncentral collisions of intermediate-energy heavy ions, *Phys. Rev. C* **65**, 064614 (2002).
- [37] R. J. Charity, $N-Z$ distributions of secondary fragments and the evaporation attractor line, *Phys. Rev. C* **58**, 1073 (1998).
- [38] D. Theriault *et al.*, Neutron-to-proton ratios of quasiprojectile and midrapidity emission in the $^{64}\text{Zn} + ^{64}\text{Zn}$ reaction at 45 MeV/nucleon, *Phys. Rev. C* **74**, 051602 (2006).
- [39] R. Vandenbosch and J. R. Huizenga, *Nuclear Fission* (Academic Press, New York, 1973).